RSC Advances

ROYAL SOCIETY OF CHEMISTRY

www.rsc.org/advances

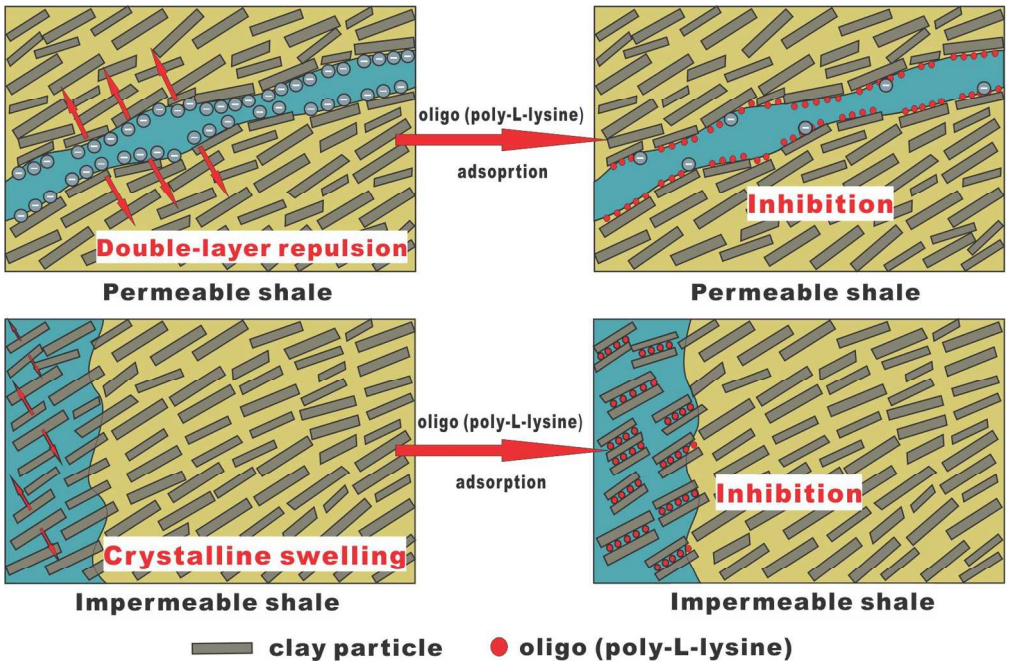

153x100mm (300 x 300 DPI)

RSC Advances

ARTICLE

Biodegradable Oligo (poly-L-lysine) as a High-Performance Hydration Inhibitor for Shale

Yang Xuan,[a] Guancheng Jiang,[a] Yingying Li,[b] Lili Yang,[a] and Xianmin Zhang[a]

Received 00th January 20xx,
Accepted 00th January 20xx

DOI: 10.1039/x0xx00000x

www.rsc.org/

Oligo (poly-L-lysine) (OPLL), utilized as a high-performance inhibitor for the hydration of shale, was synthesized with L-lysine as a monomer by the thermal copolymerization method. OPLL was characterized through Fourier-transform ion cyclotron resonance mass spectroscopy (FT-ICR-MS), nuclear magnetic resonance hydrogen spectroscopy (^{1}H NMR), Fourier-transform infrared spectroscopy (FT-IR) and Thermogravimetry (TG). The inhibition performance of OPLL was evaluated through the combination of montmorillonite (MMT) linear swelling, MMT dispersion and shale dispersion tests, and these results were compared with those for other commonly-used inhibitors in the field. The results demonstrated that OPLL possessed an outstanding inhibition effect on the hydrated dispersion of both MMT-rich and illite-rich shale that was superior to many commonly-used shale inhibitors such as KCl, 2, 3-epoxypropyltrimethylammonium chloride (EPTAC) and polyoxypropylenediamine (Jeffamine D230). Along with excellent inhibition capacity, OPLL also possessed good thermal stability and a broad pH adaptability, and therefore,it can perform well under high temperatures up to 180°C and in the pH range of 7 to 10. Based upon a combined use of X-ray diffraction (XRD) and zeta potential techniques, the inhibition mechanism was determined. The excellent performance of OPLL on shale can be attributed to the synergistic effects of the inhibition of the MMT crystalline swelling and the weakening of the diffuse double layer repulsion between clay particles. Additionally, biodegradability test proved that OPLL is an environmental friendly shale inhibitor that can be readily biodegraded.

1. Introduction

Wellbore instability, which is one of the most significant technical problems in oil and gas exploration and the largest source of lost time and revenue, has been frustrating drilling engineers for many decades.[1-4] Shales comprise 75% of all of the formations drilled by petroleum industry, and more than 90% of wellbore instability problems are caused by problematic shales.[5-7] When clay-rich shales formations are drilled in presence of water, the resulting shale hydrated swelling and dispersion can cause wellbore instability problems such as borehole enlargement, tight boreholes, stuck pipes, lost circulation, poor borehole cleaning and well control problems.[7, 8]

To address the drilling problems associated with shale instability, various kinds of drilling fluids have been developed and utilized in the field. Oil-based drilling fluids (OBFs) generally give greater shale stability than water-based drilling fluid (WBFs) system due to the prevention of water invasion into shales through a semi-permeable membrane provided by emulsifiers.[9] However, the disadvantages of OBFs such as high cost, environmental limitations, disposal problems, health and safety issues and detrimental effects on the drilling and completion of reservoir cannot be ignored.[10] Consequently, designing and developing high performance WBFs as good alternatives to OBFs has been a major goal of the petroleum drilling industry.

Because the hydration of the water-sensitive clay mineral montmorillonite (MMT) is commonly considered to be the primary cause of the shale failure, for more than the past five decades various chemicals that can inhibit clay hydration have been used in WBFs as "shale hydration inhibitors" to maintain wellbore stability.

Before the 1990's, the most widely used shale inhibitor was KCl, and most of the time it was used as the main ingredient in combination with other polymer-type species, such as partially hydrolysed polyacrylamide (PHPA)[11, 12] and polyethylene glycol (PEG)[12, 13]. The inhibition mechanism of KCl occurs via the exchange of sodium cations in the MMT interlayer with the weakly hydrating potassium cations[14, 15] However, the high concentrations of KCl that are required can seriously harm ecosystems.[16] To overcome the environmental disadvantages of KCl, alternative cation sources have been sought. Because the ammonium cation possesses a very similar hydrated volume and a similar hydration energy to the potassium cation,[17] amine-based chemicals were introduced as potent inhibitors and applied in the field during the last few decades; the most effective classes of these chemicals are quaternary ammonium salts[18-20] and polyether amines[21-25]. Despite the partial success they achieved, quaternary ammonium salts and polyether amine still have some drawbacks, such as the toxicity of some of the high-molecular-weight quaternary amine salts[26] and the relatively lower inhibition of the polyether amines. Due to these shortcomings,

[a] State Key Laboratory of Petroleum Resources and Prospecting, China University of Petroleum (Beijing), Beijing 102249, China.
[b] CNPC Drilling Research Institute, Beijing 102206, China

further efforts must be made to develop environmental friendly and high performance amine-based shale inhibitors.

Poly-L-lysine (PLL), which is a polymer comprised of lysine amino acids, has been widely utilized for biomaterial applications,[27-31] owing to its attractive properties including hydrophilicity, excellent biocompatibility and biodegradability. As a primary amine-based cationic polyelectrolyte, PLL is known to have high affinity for negatively charged substrates in a wide pH range through electrostatic attraction.[32] Therefore, it is reason to expect that PLL can act as novel biodegradable hydration inhibitor for shale. In most cases, the molecular weight of PLL that was prepared and researched in the field of biomaterial is higher than tens of thousands of grams per mole. However, high molecular weight has significant adverse effect on the shale inhibition performance, which is disclosed by studies on other cationic shale inhibitors.[21, 33]

In this paper, we synthesized oligo (PLL) (OPLL) with molecular weight less than 1000 g/mol as a high performance, environmental friendly and low cost shale inhibitor via a simple method. The inhibition performance of OPLL on the hydrated swelling and dispersion of MMT and shale was evaluated through a variety of methods, and these results were compared with those of several commonly-used inhibitors in the oil-field. Moreover, the inhibition mechanism was analysed via combined characterizations of the OPLL-MMT composites.

2. Experimental

2.1 Materials

Na-MMT with a cation exchange capacity of 72.3 mmol/100 g was provided by Xinjiang Xiazijie Bentonite Inc., China. Shale cuttings were obtained from the Sichuan oilfield in China. The raw samples of shales were characterized by X-ray diffraction, and their mineral compositions are listed in Table. 1. L-lysine hydrochloride, potassium chloride and 2, 3-epoxypropyltrimethylammonium chloride (EPTAC) were purchased from Sigma-Aldrich Inc. Polyoxypropylenediamine (Jeffamine D230, M_w 230 g/mol) was obtained from the Huntsman Corporation. The other experimental chemicals were acquired from domestic reagent companies. All of the materials were used without further purification.

2.2 Methods

2.2.1 Synthesis of OPLL. The synthesis of OPLL is based upon the thermal copolymerization method reported by M. Scholl[34] and S.W. Fox[35] with some necessary modifications. To begin the reaction, 20 g L-lysine hydrochloride and 5.8 g phosphoric acid (≥85%) were added to a 50 mL three-necked flask equipped with a PTFE stir bar and subsequently heated to 195 ℃. In the reaction process, the flask should always be kept open so that the water vapor formed during the polycondensation reaction can escape from the reactor. After an 8 h reaction time, the product in a molten state was poured out of the flask immediately before being cooling. The brownish product was taken up in dimethyl sulfoxide and the undissolved residual L-lysine monomer was filtered off. Then, the product solution was added drop-wise into a 10-fold volume of acetone under constant stirring, and the precipitated OPLL was collected by filtration under vacuum. Finally, the precipitate was dried in a vacuum oven overnight to yield the solid, yellow-brown OPLL. The product OPLL was characterized by FT-ICR MS, ^{1}H NMR, FT-IR, and TG.

2.2.2 Characterization techniques

Fourier-transform ion cyclotron resonance mass spectroscopy (FT-ICR MS). The molecular weight of OPLL was determined with an Apex Ultra 94 FT-ICR mass spectrometer (Bruker Daltonics, USA) with a standard ESI source.

Gel permeation chromatography (GPC)

The weight-average molecular weight (M_w) and number-average molecular weight (M_n), and polydispersity of the OPLL were analysed by GPC using a VISCOTEK TDA Model 300 instrument. The analysis was carried out at 35 ℃ using a 0.2 M acetic acid/0.1 M sodium acetate buffer as eluent at a flow rate of 0.5 mL/min. Sample elution was monitored with a refractive index detector.

Fourier-transform infrared spectroscopy (FT-IR). The FT-IR analyses were recorded by a Magna-IR 560 spectrometer (Nicolet, USA) with the wavenumber range of 4000-400 cm^{-1} and a resolution of 4 cm^{-1}.

Proton nuclear magnetic resonance (^{1}H NMR). ^{1}H NMR spectrum was recorded at room temperature on a Bruker Avance 400 spectrometer (Bruker, Switzerland). D_2O was used as the solvent and the spectrum was calibrated using the residual protons of the solvent.

Transmission electron microscopy (TEM). The TEM analyses were performed by a JEM-2100 transmission electron microscope (JEOL, Japan). The samples were prepared by dipping the prepared aqueous dispersion onto the amorphous carbon-coated copper TEM grids and dried under an infrared lamp.

Thermogravimetry (TG). TG analyses were obtained through the utilization of a NETZSCH STA 409 PC/PG (Bayern, Germany) at a heating rate of 10 ℃/min from 25-800 ℃ in a high-purity Ar atmosphere.

X-ray diffraction (XRD). The XRD patterns of the OPLL-MMT composite samples were obtained using a Panalytical X'pert PRO diffractometer (PANalytical, Netherlands) with Cu Kα radiation (λ = 1.5406 nm) operated at 40 kV and 40 mA. Diffraction patterns were collected with 2θ angle scanning between 3 °and 15 °.

Zeta potential measurements. The zeta potentials of the MMT suspensions were determined using a Zetasizer Nano ZS instrument (Malvern, U.K) at 25 ℃. The equipment measures the electrophoretic mobility of the particles and converts that mobility to the zeta potential using the Smoluchowski equation. Different inhibitors were mixed with the MMT suspensions to obtain 0.1 wt% MMT suspensions with different inhibitor concentrations. The suspensions were shaken for 16 h at room temperature and then allowed to settle for 2 h. After settling, the zeta potentials of the supernatants were measured.

Table. 1. Mineral compositions of the experimental shales

Samples	Quartz	Total clay	% by weight of the total clay				
			Montmorillonite	Illite	Kaolin	Mixed layer Illite/Montmorillonite	%Montmorillonite in mixed layer
Shale 1#	47	26	--	31	3	62	55
Shale 2#	34	24	--	41	2	46	20

2.2.3 MMT linear swelling tests. The degree of swelling of the compacted MMT immersed in different inhibitor solutions were determined in the laboratory utilizing a CPZ-2 dual channel linear swellmeter (Qingdao, China). A sample of 5 g MMT was grounded, passed through a mesh with a pore size of 48 μm and then compressed into a sized pellet through a hydraulic press with a pressure of 10 MPa for 5 min. The pellet was then placed between a metal plate and a linear transducer. After immersing the pellet in the inhibitor solution in which the pH was adjusted to 9 via the addition of NaOH, the change in the length of the pellet was measured under a measurement rate of 30 s through the transducer. Both the total change in length over the whole experimental time frame and the rate of change within a certain period could be determined.

2.2.4 MMT dispersion tests. The MMT dispersion test aims at evaluating the inhibition effect of the shale inhibitor on the hydrated dispersion of MMT. Different amounts of MMT were added to 300 g of deionized (DI) water or the inhibitor solution at a concentration of 1 wt%. After high-speed stirring at room temperature for 30 min, the yield point of the MMT/inhibitor suspension was determined.

For the MMT dispersion tests at a constant MMT loading and variable pH values, the concentration of MMT was fixed at 16 wt%, and the pH value of the suspension ranged from 7-11.

The measurements were obtained using a ZNN-D6L rotational viscometer (Qingdao, China). The yield point and plastic viscosity of the MMT/inhibitor suspension was calculated from viscometer readings of 600 and 300 rpm (Φ600 and Φ300) using the following formulas:

Yield point (YP) = Φ300-Φ600/2 (Pa).

Plastic viscosity (PV) = Φ600-Φ300 (mPa.s)

2.2.5 Shale dispersion tests. In this test the loss of dispersed shale after a period of hydration was determined gravimetrically. 20 g shale cuttings with 6-10 mesh sizes was hot rolled in 300 mL DI water or inhibitor solutions (pH adjusted to 9) at 120 ℃ for 16 h. After cooling down, the remaining cuttings were screened using a 40 mesh sieve and washed with 10 wt% NaCl solution. Then the cuttings retained on the sieve was dried at 105 ℃ and then weighed to obtain the recovery percentage.

2.2.6 Preparation of the OPLL-MMT composite. OPLL aqueous solutions were prepared at different concentrations, and the pH values of solutions were adjusted to 9 with 1 M NaOH (using pH meter). Then, 9 g of MMT was dispersed in 291 g of the OPLL solution to make a 3 wt% OPLL/MMT suspension. The suspensions were stirred vigorously at 10000 rpm for 20 min and then hot rolled at 80 ℃ for 16 h to reach the adsorption and hydration equilibrium. After being cooled to room temperature, the suspensions were centrifuged at 8000 rpm for 10 min, and the solid samples were washed with DI water to eliminate the residual OPLL solution. The washing and centrifugation processes were repeated several times until the pH value of supernatant was approximately 7. Finally, the solid composites were dried overnight at 105 ℃ and ground to fine powders for the use in the XRD, FT-IR and TG analyses.

2.2.7 Biodegradability tests. The biodegradability of OPLL was measured as ratio of the chemical oxygen demand (COD) and the biochemical oxygen demand (BOD). The COD determination was made using the potassium dichromate oxidation method, and the BOD determination was determined using an iodometric method.[36]

3. Results and discussion

3.1 Characterizations

3.1.1 Molecular weight determination. The weight-average (M_w) and number-average (M_n) molecular weight of the OPLL obtained by GPC were 692 g/mol and 445 g/mol respectively, and the polydiversity index (M_w/M_n) was calculated to be 2.024 (spectrum not shown). To determine the exact molecular weight of the synthesized OPLL, FT-ICR MS was used in combination with GPC. Fig. 1 shows the FT-ICR mass spectrum of OPLL, from which it can be observed that its molecular weight is generally in the range of 200-1000 g/mol. In the spectrum, three

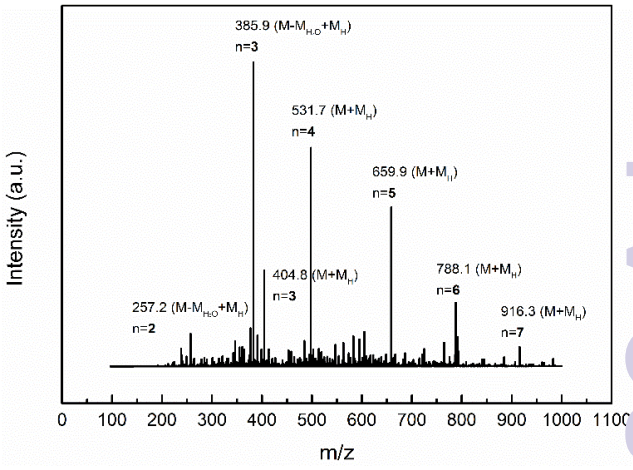

Fig. 1. FT-ICR mass spectrum of OPLL.

pseudo molecular ion peaks with high intensities are located at m/z values of 385.9, 531.7 and 659.9, corresponding to the molecular weights of 402.6 g/mol, 530.7 g/mol and 658.9 g/mol, respectively. This suggests that most of the as-synthesized OPLL molecules were trimers, tetramers and pentamers.

3.1.2 FT-IR spectra of OPLL and the OPLL-MMT composite. Fig. 2 presents the FT-IR spectra of L-lysine, OPLL, MMT, and the OPLL-MMT composite. In the L-lysine spectrum, the broad peak at 2943 cm^{-1} and shoulder peak at 1457 cm^{-1} can be assigned to the stretching and deformation vibrations of the CH_2 group.[37] The peaks at 1628 cm^{-1} and 1499 cm^{-1} represent the stretching vibration of the COO^- group and NH_3^+, respectively.[37] For the OPLL spectrum, two new peaks emerged at 1665 cm^{-1} (amide I band) and 1516 cm^{-1} (amide II band),[38] indicating the polycondensation of L-lysine via the amidation of the carboxyl groups.

The FT-IR patterns of the MMT exhibited the extremely typical characteristic of smectite group. Some of the major absorption peaks were the following: stretching bands of the structural O-H (3625 cm^{-1}), the broad stretching band of the physisorbed water (3425 cm^{-1}), the deformation band of water (1639 cm^{-1}), bands of Si-O stretching and Si-O-Si bending (1040 cm^{-1} and 1080 cm^{-1}), deformation bands of Al-Al-OH vibrations (917 cm^{-1}), coupled out-of-plane vibration band of Al-O and Si-O (625 cm^{-1}) and deformation bands of Al-O-Si and Si-O-Si, located at 521 cm^{-1} and 465 cm^{-1}, respectively.[39] In the case of the OPLL-MMT composite, although the peaks that are attributed to the amide group in OPLL cannot be distinguished, the peak that appeared at 1457 cm^{-1} (CH_2 stretching bands) undoubtedly suggests the adsorption of OPLL on the MMT surface. Additionally, the spectrum also possess broad and weak peaks at 3425 cm^{-1} and 1639 cm^{-1}, indicating a significant decrease in the interlayer water.

3.1.3 ^{1}H NMR spectrum of OPLL. OPLL is a polycondensation product of the amino acid L-lysine, which contains two amino groups (α-amino and ε-amino). As reported

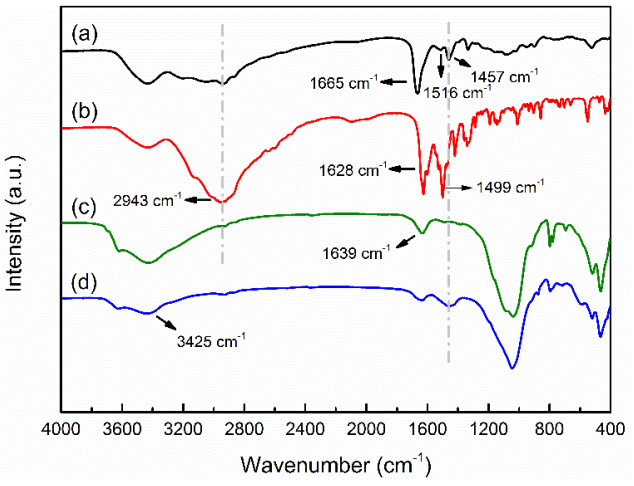

Fig. 2. FT-IR spectra of (a) OPLL, (b) L-lysine, (c) MMT and (d) OPLL-MMT composite.

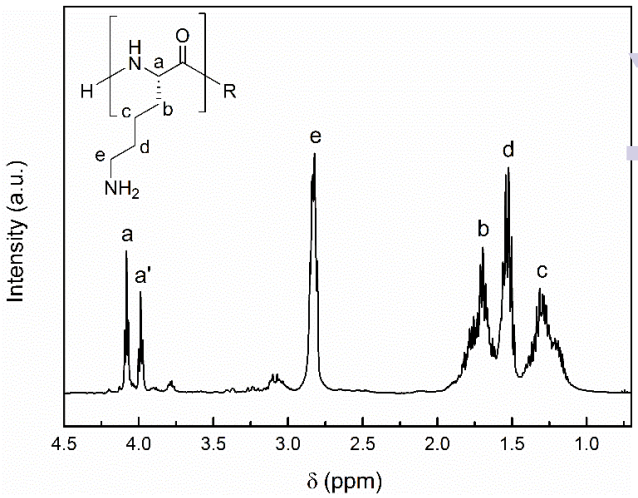

Fig. 3. ^{1}H NMR spectrum of OPLL.

in the literature,[34] due to the higher reactivity of the ε-amino group of the monomer, the mole fraction of the ε-linked linear units was far greater than that of the α-linked units in the hyperbranched poly(L-lysine) structure that was thermally polymerized using a metal-based amidation catalyst, such as $Zr(O^nBu)_4$ and $Ti(O^nBu)_4$.

The microstructure of the OPLL was characterized by the ^{1}H NMR spectrum, which is shown in Fig. 3. The peak at 4.08 ppm in the spectrum was assigned to the α-CH proton of the α-linked lysyl units, and the near peak at 3.98 ppm originated from the α-CH proton of the terminal lysyl units[40]. The three broad peaks located in the range of 1.2 ppm-1.8 ppm were attributed to the β, γ and δ-CH_2 groups. The highest peak at 2.82 ppm was assigned to the ε-CH_2 group next to a free amino group.[34, 40] Additionally, no signals that can be attributed to the α-CH proton or the ε-CH proton of the ε-linked lysyl units were apparently visible, indicating that the OPLL synthesized in this paper was mainly composed of α-linked units. This finding could be due to that, in the presence of phosphoric acid as catalyst, the L-lysine monomers have a strong tendency to polymerize via the amidation of the α-NH_2 group rather than the ε-NH_2 group.

3.2 Inhibition performance on the MMT and shale

3.2.1 MMT linear swelling tests. The linear swelling curves of the compacted MMT that was immersed in DI water, OPLL and other inhibitor solutions of the same concentration are presented in Fig. 4. For all of the samples, the swelling curves displayed a similar shape with a strong increase within the initial period of time followed by a relatively slower growth, exhibiting typical swelling behaviour of MMT in aqueous solution. Within the experimental time frame, the linear swelling height of the MMT in DI water was the highest amongst all of the samples. Compared with that in DI water, the extent of swelling of the MMT in the OPLL, KCl, EPTAC and Jeffamine D230 solution was reduced by 38%, 29%, 28% and 8%, respectively. These differences suggest larger inhibition of the OPLL on the MMT swelling compared to that of the other inhibitors.

The linear swelling behaviour of compacted MMT in aqueous media is strongly dependent on the crystalline swelling that

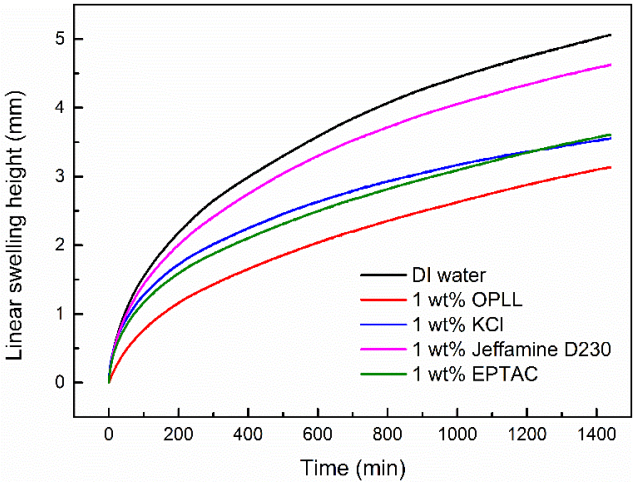

Fig. 4. Linear swelling curves of the MMT in DI water, OPLL and other inhibitor solutions.

occurs between the individual MMT layers caused by the hydration of interlayer cations and layer surfaces.[41] Therefore, the stronger inhibition of OPLL on swelling of compacted MMT could be mainly due to the higher inhibition on crystalline swelling of the MMT.

3.2.2 MMT dispersion tests. Investigating the rheology of MMT/inhibitors suspensions is an effective way to evaluate the inhibition performance on the MMT hydrated dispersion. The yield point of the suspension reflects the intensity of the internal network structure formed by the dispersed MMT particles in laminar flow. A higher yield point indicates a higher particle number and a stronger network structure and, conversely, a weaker inhibition on the dispersion of MMT particles. The yield points of the MMT/OPLL suspensions as a function of the MMT dosage are shown in Fig. 5. Obviously, the inhibition on MMT dispersion is influenced by OPLL concentration. The extent of the dispersion was higher in the lower concentration solutions

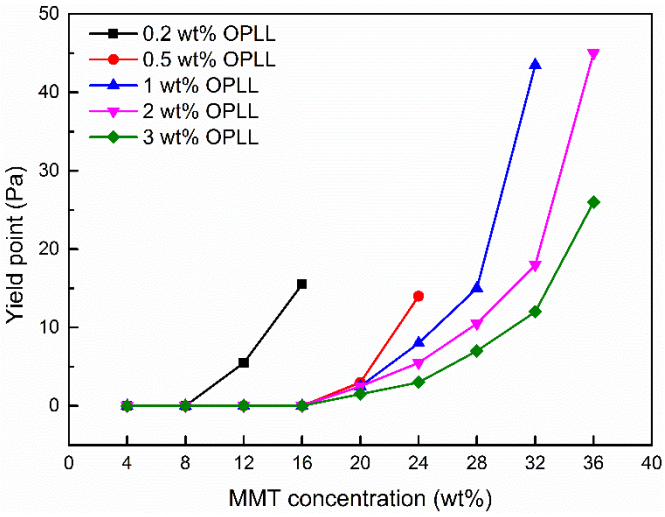

Fig. 5. Yield points of the MMT/OPLL suspensions as a function of MMT concentration.

than in higher ones due to the lower amounts of OPLL that were adsorbed onto the MMT particles. With increasing MMT concentrations, the yield points increased for all of the samples, and the gaps between the yield points also gradually enlarged. At the low MMT concentrations, only small amounts of the OPLL molecules are required to reach the saturated adsorption on MMT, thus leading to a similar inhibition performance of the OPLL with different concentrations. However, at relatively higher MMT concentrations, the low inhibition of samples with low OPLL concentrations are much more distinct due to the lower amounts of OPLL molecules that were available to adsorb onto the MMT.

The difference in dispersion states of the MMT in pure water and OPLL solution can be directly observed by TEM, as shown in Fig. 6. Apparently, the plate-like MMT particles dispersed in OPLL solution is much thicker and longer than in DI water, indicating that the dispersion of the MMT particles is inhibited by OPLL. The size of MMT particles in aqueous suspension is mainly governed by the diffuse double layer repulsion.[42] If the repulsion between the diffuse double layers of two approaching MMT particles is weak enough to be overcome by kinetic energy, the diffuse portions of the double layers will begin to fuse, which results that the two particles join together forming one larger particle. The reduction of particle number undoubtedly has an adverse effect on the formation of network structure, as indicated

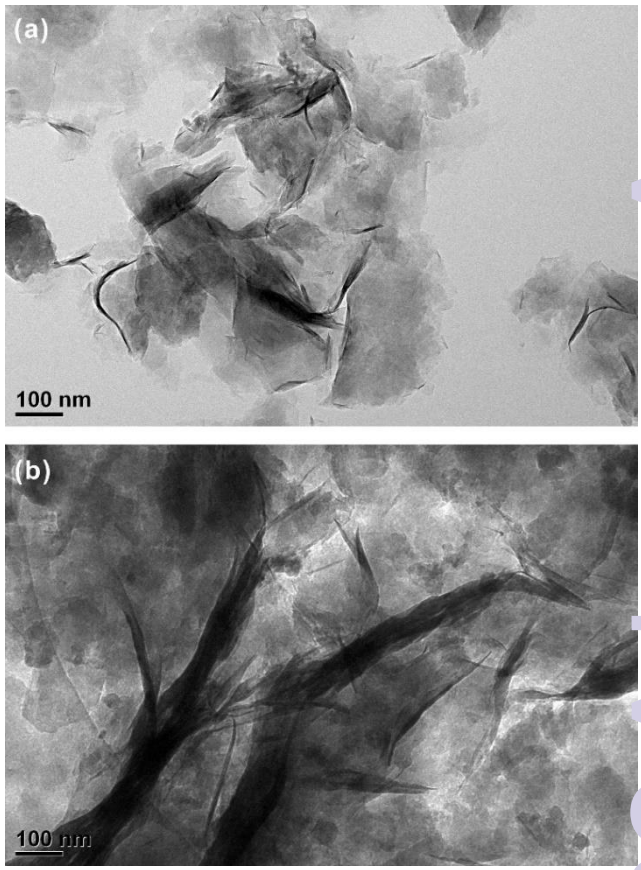

Fig. 6. TEM images of the MMT dispersed in (a) DI water and (b) 1 wt% OPLL solution.

by the decrease in the yield point of suspension. Consequently, the inhibition on hydrated dispersion of MMT particles by OPLL could be attributed to the weakening of the double-layer repulsion through electrostatic neutralization between the negative MMT surface and the positive charged OPLL. The detailed analysis will be discussed in the later section.

Electrostatic attraction between the positively charged amine groups and the negative MMT surface and ion exchange with interlayer cations are the main driving forces for the adsorption of the OPLL molecules onto the MMT particles. Only when the pH value of solution is close to or lower than the pK_a value of OPLL can the protonation of amine groups occur. Therefore it can be expected that the inhibition performance of the OPLL would be strongly influenced by the pH value of solution. Fig. 7 shows the yield points and the plastic viscosities of the MMT/OPLL suspensions as a function of pH with the same MMT concentration. In the pH range between 7 and 10, the yield points and the plastic viscosities did not exhibit an obvious change. However, when the pH value increased to 11, these two values simultaneously possessed a significant increase, indicating the poor inhibition on the dispersion of the MMT particles. Therefore, it can be deduced that the pK_a value of OPLL is in the range between 10 and 11. The fact that the reported pK_a of ε-NH_2 and α-NH_2 in poly(L-lysine) is 7.6[43] and 10.5[44], respectively, further proves that the OPLL synthesized in this paper was predominantly of the α-type. This test suggests that the OPLL can exhibit a good performance in the WBFs, where the pH range is generally fixed between 9.5 to 10.5.[45]

The inhibition capacity at high temperature is also of great significance for the shale inhibitor because the drilling depth in the recent decades is much deeper than ever, and therefore, the inhibitor needs to be able to overcome the negative effects brought about by high temperatures. Fig. 8 presents the yield points of the MMT/OPLL suspensions as a function of temperature with the same MMT concentration. In the temperature range between 90 ℃ to 180 ℃, no significant change in the yield point and plastic viscosity was detected for

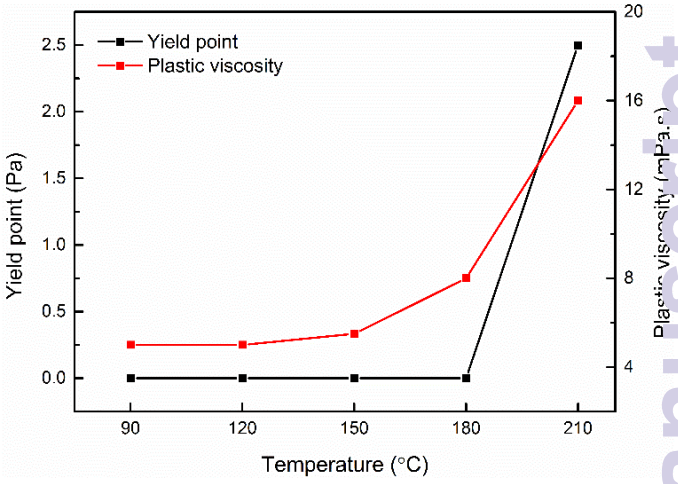

Fig. 8. Yield points and plastic viscosities of the MMT/OPLL suspensions as a function of temperature

the MMT/OPLL suspension. However, when the temperature was further increased to 210 ℃, both of the two values increased sharply, indicating the serious weakening of the inhibition performance of OPLL under such a high temperature.

Fig. 9 presents the TG curves of the OPLL, pristine MMT and the OPLL-MMT composite. For OPLL, within the experimental temperature range, there are two major stages in the process of thermal decomposition. The slight weight loss from 30 ℃ to ~120 ℃ was attributed to the evaporation of the physically adsorbed water. The second stage began at approximately 250 ℃ and a rapid loss of weight up to 50 wt% was observed; this effect was attributed to the thermal decomposition of the unstable functionalities, such as the primary amine and amide. Because the thermal decomposition of OPLL will not occur when the temperature is lower than 250 ℃, the poorer inhibition performance on MMT dispersion at 210 ℃ could be due to the significantly weakened electrostatic adsorption of OPLL on the MMT surface at the high temperature.

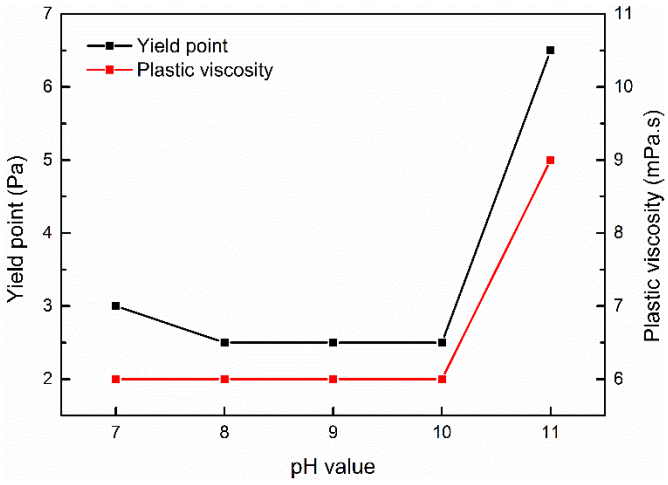

Fig. 7. Yield points and plastic viscosities of the bentonite/OPLL suspensions as a function of pH.

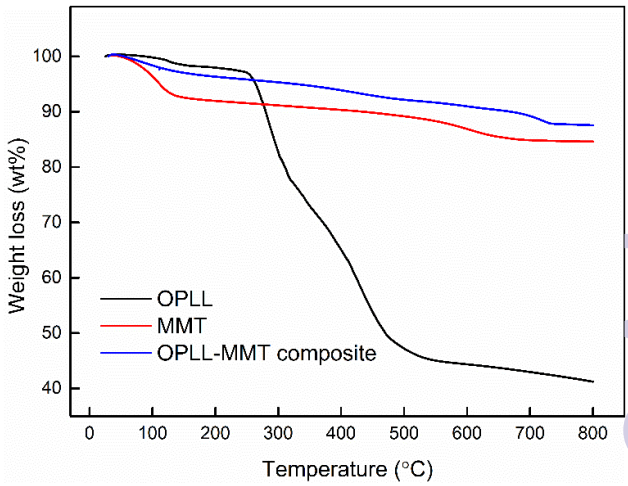

Fig. 9. TG curves of the OPLL, pure MMT and OPLL-MMT composite.

In the case of pristine MMT, the mass loss step observed up to ~140 ℃ was ascribed to the release of the free (interstitial water and surface adsorbed water) and interlayer water. The second step, starting from ~550 ℃, due to the removal of the structural water (bonded hydroxyl moieties that underwent dihydroxylation).[46] The TG curve of the OPLL-MMT composite demonstrated that the amount of free and interlayer water in MMT decreases after the adsorption of the OPLL molecules, indicating the effective inhibition of the OPLL on the hydration of MMT.

Fig. 10 compares the inhibition performance of the OPLL with other commonly-used inhibitors, including KCl, Jeffamine D230 and EPTAC. Apparently, at the same concentration, the yield point of the MMT/OPLL suspension was much lower than that of any other inhibitor, indicating the higher inhibition of OPLL on the MMT hydrated dispersion.

3.2.3 Shale dispersion tests. Two shale samples of different clay compositions were used in the evaluation of the inhibition performance of the OPLL. The recovery percentage of the shale cuttings with relatively high MMT contents (shale 1#) after they were hot-rolled in DI water, OPLL and other inhibitor solutions are presented in Fig. 11. The curves for all of the samples possessed similar trends, with the recovery percentage increasing significantly at low concentrations and reaching a quasi-plateau at higher concentrations; this pattern indicated that the adsorption of the inhibitor molecules on the clay minerals in the shale was near the saturation point. At the same concentration, the recovery percentage of the shale cuttings in the OPLL solution was always the highest amongst all of the tested inhibitors and approached 78 wt% for the concentration of 3 wt%. The performances of the other inhibitors were much poorer than that of OPLL in the shale dispersion tests. Additionally, it should be noted that in this test, Jeffamine D230 possessed a better inhibition on the shale dispersion than EPTAC, whereas in the MMT dispersion tests, the result was just the opposite. This difference could be due to the "cloud point" effect[47] that improved the inhibition of Jeffamine on the shale dispersion.

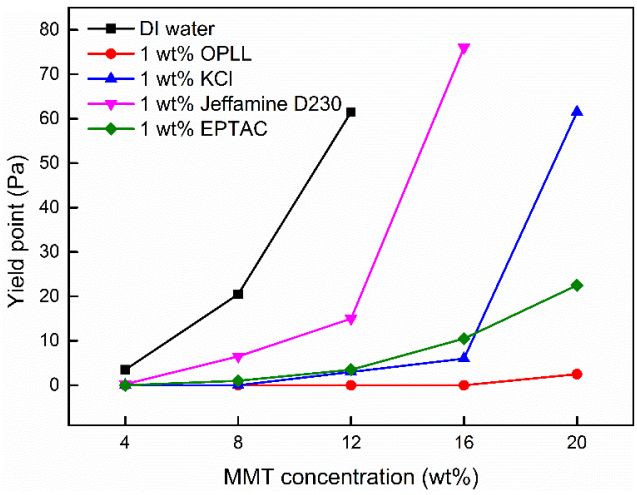

Fig. 10. Yield points of the MMT/inhibitors suspensions as a function of MMT concentration.

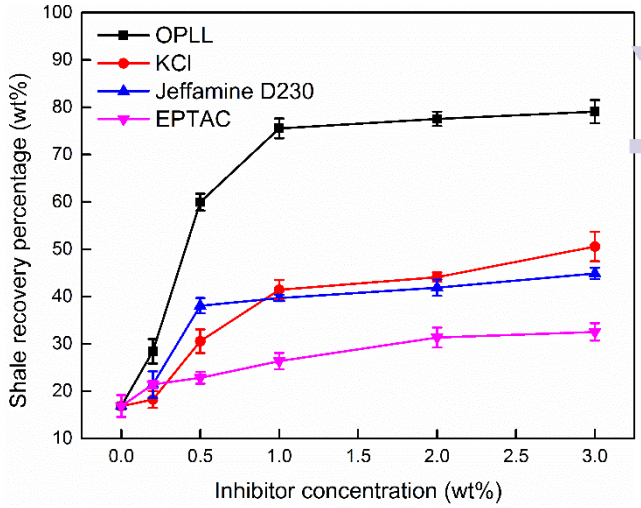

Fig. 11. Recovery percentages of the shale with a relatively high MMT content after being hot-rolled in different inhibitor solutions at 120 ℃ for 16 h.

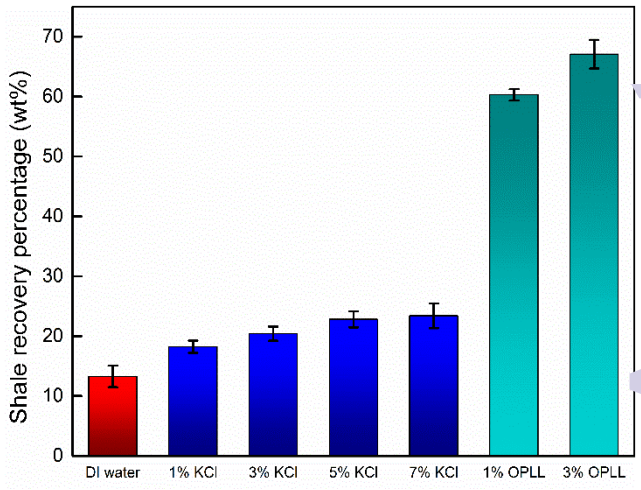

Fig. 12. Recovery percentages of the shale with relatively high illite contents after being hot-rolled in KCl and OPLL solutions at 120 ℃ for 16 h.

Above the cloud point temperature (~50 ℃), the Jeffamine solution started to phase separate. The droplets or aggregates resulting from the separation of the Jeffamine-rich phase can seal the shale surface, thereby reducing the water ingress into the shale.[48]

Although the traditional inhibitor KCl has a strong inhibitory effect on the swelling of MMT, it had hardly any effect on the non-swelling minerals, such as illite, according to a report by Van Oort.[3] Fig 12 shows the recovery percentages of the shale with relatively high illite contents (shale 2#) after they were hot-rolled in DI water, KCl or OPLL solutions. The recovery percentage in DI water was 13 wt%, and the value was merely increased to 23 wt% by the KCl solution with up to 7 wt% concentration, which indicated the negligible inhibition of KCl on the illite-based shale. In sharp contrast, the shale recover

percentage was increased significantly to 59 wt% by the 1 wt% OPLL solution. This difference suggests that OPLL can effectively inhibit the hydrated dispersion of both the MMT-rich and illite-rich shale.

3.3 Inhibition mechanism analysis

So far, there is no uniform view about the role of clay mineralogy in relation to the shale instability. The most often cited explanation emphasizes a volume expansion following the osmotic swelling of the interlayer space of MMT as the primary failure mechanism.[3] However, in a recent paper,[49] Wilson and Wilson argued that this mechanism could not account for the instability of illite-rich or kaolin-rich shales and that it was not at all certain that it was necessarily applicable to all MMT-rich shales. They maintained that the swelling and dispersion of shales envisaged a combined mechanism of the crystalline swelling of MMT and the overlap of the diffuse double layers of negatively charged clays (MMT, illite or kaolin). When the impermeable shale with high clay contents came into direct contact with the drilling fluid at the exposed wellbore face, shale swelling may occur through the crystalline expansion of MMT. As for the more permeable shales with high proportions of non-clay minerals, the drilling fluid invaded into the intra-aggregate pores more rapidly than to the interlayer space of the MMT. In this scenario, the failure of shale was related to the overlap of the diffuse double layers associated with the charged external surfaces of the clay minerals exposed in opposing walls of micro- and meso-pores of the shale, thereby leading to a build-up of pore pressure. In this upcoming section, the inhibition mechanism of OPLL on the shale destabilization was analysed based upon Wilson's theory.

3.3.1 Effect of OPLL on crystalline swelling. XRD was used to investigate the changes in the interlayer spacing (d_{001}) of OPLL-MMT composite compared with pristine MMT, from which the inhibitory effect on the crystalline swelling of MMT could be evaluated.

Fig. 13(a) presents the XRD patterns of the dry OPLL-MMT composites with different OPLL concentrations. The peaks were assigned to the (001) basal diffraction of the MMT. It was observed that the pristine MMT exhibited broad diffraction peak at $2\theta=8.8°$, which corresponded to an average interlayer spacing of 9.74 Å, revealing a dominant dehydrated interlayer stage.[50] The addition of small amounts of OPLL immediately modified the XRD patterns. For a low concentration of 0.2 wt% OPLL, the peak shifted toward the lower angle side corresponding to interlayer spacing of 13.1 Å. As the concentration of OPLL increased to above 0.6 wt%, the interlayer spacing further expanded to 13.6 Å, which is the sum of the thickness of dehydrated MMT and a single layer of OPLL molecules. This effect indicated the successful intercalation of the OPLL into the interlayer of MMT driven by cationic exchange.[51]

In addition, with an increase in OPLL dosage, the diffraction patterns exhibited a significant increase in the crystallinity as judged from the half width of the d_{001} signals. Higher crystallinity indicates a greater inhibition on the hydrated dispersion of the MMT quasicrystals with higher OPLL concentrations.[4] For the concentrations of OPLL above 1.5 wt%,

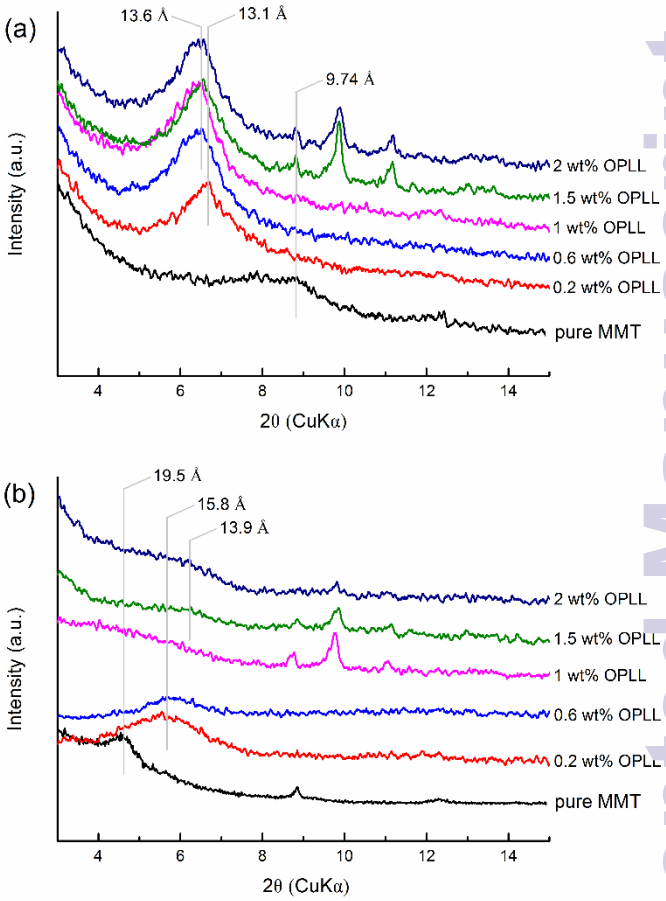

Fig. 13. XRD patterns of (a) dry OPLL/MMT composites and (b) wet OPLL/MMT composites with different concentration of OPLL.

the patterns distinctly demonstrated two peaks, thus revealing a coexistence of layers with and without intercalation with the OPLL molecules. This pattern suggests that some of the layers were intercalated before the others, which may be linked to the layer charge heterogeneities that are nearly always present in natural swelling clays.[52]

The evolution of the XRD patterns of the wet OPLL-MMT composites with the concentration of OPLL is presented in Fig 13(b). For pristine MMT, the XRD pattern displayed an interlayer spacing of 19.5 Å, corresponding to a dominant three-layer hydrate stage of MMT.[53] With the increase in the OPLL concentration to 1.5 wt%, the interlayer spacing gradually decreased to 13.9 Å, and the further increase of concentration to 2 wt% did not obviously change the spacing. It must be noted that this value was approximately the same as that of the dry OPLL-MMT composite (13.6 Å), which may indicate that the intercalated OPLL molecules almost totally prevented any crystalline swelling resulted from the uptake of water.

Our previous studies have shown that the degree of crystalline swelling was closely correlated with the macroscopic swelling degree of the densely compacted MMT immersed in inhibitor solution,[54] which is also clearly revealed in Fig. 14. This figure compares the macroscopic linear swelling height and the

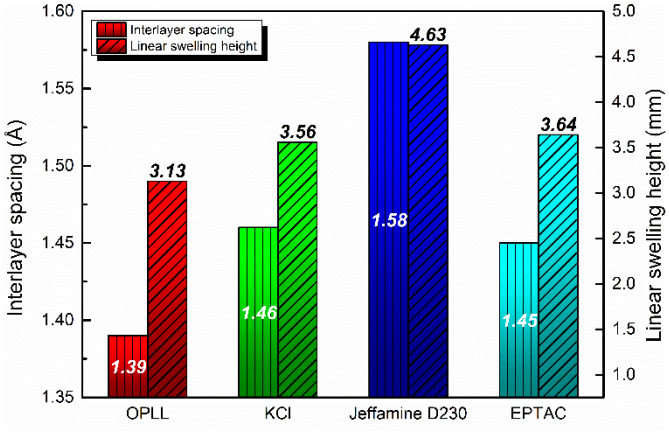

Fig. 14. Swelling degree of the MMT in different inhibitor solutions (diagonal stripe bars) and the interlayer spacing of the wet inhibitor-MMT composites (vertical stripe bars).

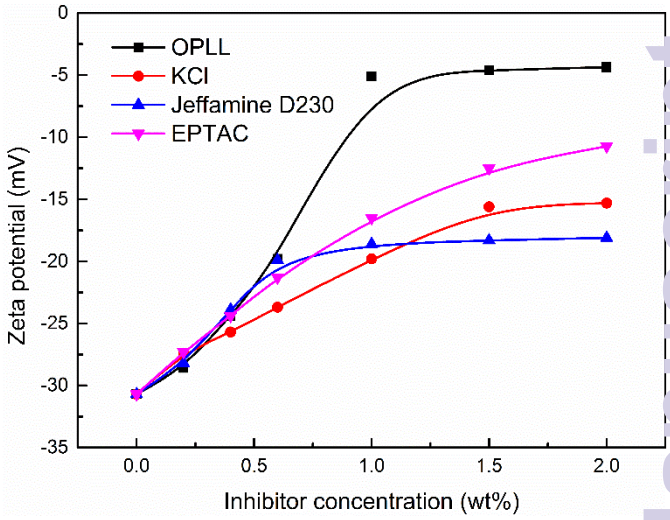

Fig. 15. Zeta potential of the MMT colloidal particles dispersed in different inhibitor solutions

microscopic change in the interlayer spacing of the MMT exposed to different inhibitor solutions. It can be observed that the MMT sample, which had a lower degree of macroscopic swelling in the OPLL solution, shows a smaller interlayer spacing than what was observed with other inhibitor solutions. This finding indicated that OPLL effectively inhibited the hydrated swelling of MMT-rich shale via intercalating into the interlayer space and preventing the crystalline swelling of MMT. Additionally, it is worth mentioning that the MMT sample that was compressed under an applied stress of 15 MPa for the linear swelling test was dense enough to approximately represent impermeable shale with a high MMT content.[49] Therefore, it can be concluded that inhibiting crystalline swelling of MMT is an effective way for OPLL to prevent the impermeable shale from destabilizing.

3.3.2 Effect of OPLL on double-layer repulsion. Zeta potential measurements were performed for investigating the effects of OPLL on the repulsive double-layer interactions between MMT particles. Fig. 15 presents the zeta potential of the MMT particles dispersed in different inhibitor suspensions as a function of the inhibitor concentration. The zeta potential of the pristine MMT is ~30 mV, indicating a favorable dispersion in water. It appears that for all of the samples, the zeta potential was less negative with an increase in the inhibitor concentration until a quasi-plateau was reached. At low concentrations, there were tiny differences in the zeta potential for the different inhibitors, whereas with the increase in concentration, the distinction become quite significant, indicating the different adsorption affinities for MMT for these inhibitors. At the quasi-plateau, the zeta potential of MMT dispersed in the OPLL solution approached ~-4 mV, which was much closer to 0 mV compared with the potentials observed with KCl, Jeffamine and EPTAC.

For all three of the cationic inhibitors, including OPLL, the zeta potential did not reverse to a positive value, indicating the adsorption amount was lower than the CEC of MMT. The adsorption of the low molecular weight cationic polymer below the CEC is mainly due to the electrostatic interactions, and the adsorption above the CEC is due to additional hydrophobic interactions between the adsorbing molecular chains.[55] Because OPLL does not possess long hydrophobic alkyl chains, the adsorption on the MMT cannot result in the inverse of zeta potential, which may re-stabilize the diffuse double layers. The zeta potential values of the MMT in different inhibitor solutions was extremely consistent with the inhibition effects on MMT hydrated dispersion. Crystalline swelling is a process that occurs within the individual layers; whereas in contrast, double-layer swelling is a process that occurs between the colloidal particles,[42] which is the main reason behind the stable dispersion of the MMT in aqueous media. The comparison of Fig. 9 and Fig. 14 showed that the inhibitor that can neutralize the negative charge on the MMT surface to the greatest extent had the best inhibitic on MMT dispersion, and this can be attributed to the decrease of the surface charge potential and the resulting extreme weakness of the double-layer repulsion. As previously mentioned, for more permeable shale, the double-layer repulsion associated with the charged external surfaces of the clay particles exposed in the opposing walls of shale pores is considered to be the dominant factor causing dispersion.[49] Therefore, the ability to effectively weaken the double-layer repulsion between clay particles undoubtedly ensures the high inhibition performance of OPLL on permeable shale, no matter the main clay mineral in the shale is MMT or non-swelling type, such as illite and kaolin.

According to the opinion of Wilson and Wilson,[49] generally, the hydrated dispersion of shale may be influenced by both the crystalline swelling and the double-layer repulsion of clay. Thus it is reasonable to speculate that the high inhibition performance of OPLL on shale is owning to its outstanding ability to inhil crystalline swelling of MMT and weaken double-layer repulsive interaction between clay particles. The probable mechanism of shale inhibition by OPLL is shown in Fig. 16.

3.4 Cost and environmental aspects

In addition to the high performance on shale inhibition, oth r advantages of the OPLL are its very good environmental compatibility and low production cost. L-lysine is useful as

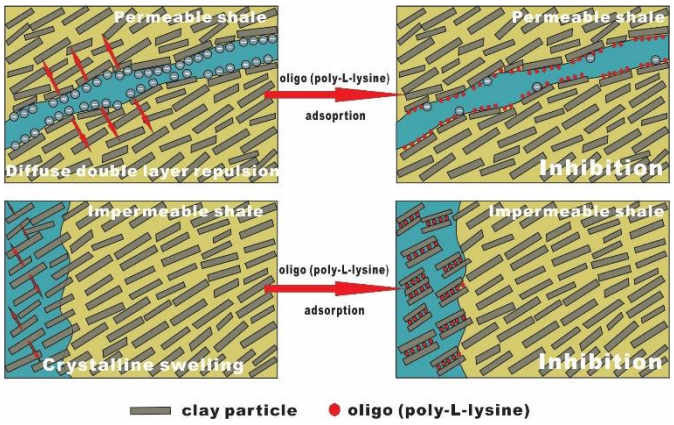

Fig. 16. Schematic diagram of the shale inhibition by OPLL.

medicament, chemical agent, food material (food industry) and feed additive (animal food), and its demand has been steadily increasing in recent years; several hundred thousand tons of L-lysine (approximately 800,000 tons/year) are annually produced worldwide almost always by microbial fermentation.[56] In china, the average price of feed grade L-lysine (98%) is only about $1,400/ton; therefore, OPLL is expected to be economically viable for use in drilling industry.

Biodegradability and non-toxicity are of great importance to drilling fluid additive because of the tightening of environmental regulations. BOD/COD_{Cr} constitutes a good measure of the biodegradability of chemicals. Fig. 17 shows the changes in the BOD/COD_{Cr} ratio of OPLL over time. According to the general principle for determining biodegradability,[57] organic matter with a ratio of $BOD/COD_{Cr} > 0.6$ on the 28th day can be deemed to be easily biodegradable. From Fig. 17, it can be observed that the BOD/COD_{Cr} value of OPLL within 5 days has already reached a value of 0.65, indicating that OPLL can be thoroughly biodegradable after a short period of time and therefore beneficial in protecting the environment. Additionally, as reported in the literature,[58] polylysine and its derivatives with

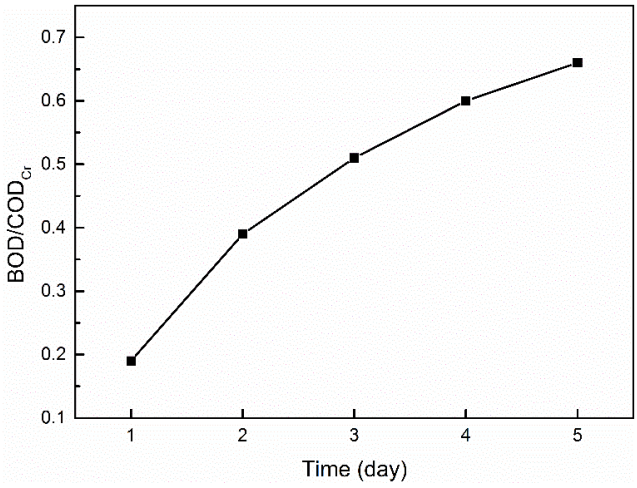

Fig. 17. BOD/COD_{Cr} curve of OPLL over time

similar structures are non-toxic. Therefore, due to the high biodegradability and non-toxicity, OPLL can be applied as a promising environmental friendly shale inhibitor in WBFs that could be used in both onshore and offshore drilling.

4. Conclusions

The synthesis, characterization and evaluation of oligo (poly-L-lysine) (OPLL) was performed to determine its feasibility as a biodegradable high-performance inhibitor for the hydration of shale. FT-ICR mass spectrum proved that the OPLL molecules were mainly trimers, tetramers and pentamers. The results of ^1H NMR analysis suggests that the OPLL molecules were mainly composed of α-linked lysyl units formed through the polycondensation of α-amino groups and carboxylic acids.

The MMT linear swelling and dispersion tests exhibited high inhibition of OPLL on hydration of MMT, superior than many commonly-used inhibitors in the field. Additionally, FT-IR and TG characterizations on the OPLL-MMT composite demonstrated that the amount of free and interlayer water in the MMT significantly decreased after the adsorption of OPLL, further indicating the effective inhibition of the OPLL with respect to MMT hydration. The results of shale dispersion tests suggested that the OPLL could efficiently inhibit the hydrated dispersion of not only the MMT-rich but also the illite-rich shale. This finding represents a significant advantage over the traditional inhibitor KCl, which possesses an extremely limited inhibitory effect on illite-rich shale. In addition to strong inhibition performance, the OPLL also possesses good thermal stability, broad pH adaptability and favorable biodegradability, which ensures that OPLL can be utilized as a promising environmental friendly shale inhibitor in water-based drilling fluid.

The inhibition mechanism of OPLL was determined based on the combined use of XRD and zeta potential techniques. The results of the XRD analysis demonstrated that OPLL can intercalate into the interlayer of MMT, and therefore prevent crystalline swelling to a great extent. Zeta potential analysis demonstrated that OPLL can effectively neutralize the negative charge on the MMT surface and thereby significantly weaken the double-layer repulsion between MMT particles. Therefore, it can be concluded that the excellent inhibitive performance of OPLL on shale can be attributed to the synergistic effects of the inhibition of the MMT crystalline swelling and the weakening of the double-layer repulsion between clay particles.

Acknowledgements

We would like to thank the following for their financial support for this work: the National Natural Science Foundation of China (No. 51474231), the Foundation for Innovative Research Groups of the National Natural Science Foundation of China (No. 51221003) and the National High Technology Research and Development Program of China (2013AA064803).

References

1 G. Chen, M. E. Chenevert, M. M. Sharma and M. Yu, *J. Pet. Sci. Eng.*, 2003, **38**, 167-176.
2 M. E. Zeynali, *J. Pet. Sci. Eng.*, 2012, **82**, 120-124.
3 E. Van Oort, *J. Pet. Sci. Eng.*, 2003, **38**, 213-235.
4 Y. Xuan, G. Jiang, Y. Li, J. Wang and H. Geng, *Colloids Surf., A*, 2013, **422**, 50-60.
5 T. Sensoy, presented in part at the SPE Annual Technical Conference and Exhibition, New Orleans, Louisiana, October, 2009.
6 E. Van Oort, A. H. Hale, F. K. Mody, S. Roy, *SPE Drill. Completion*, 1996, 137-146.
7 M. Lal, presented in part at the SPE Asia Pacific Oil and Gas Conference and Exhibition, Jakarta, Indonesia, April, 1999.
8 R. L. Anderson, I. Ratcliffe, H. C. Greenwell, P. A. Williams, S. Cliffe and P. V. Coveney, *Earth-Sci. Rev.,* 2010, **98**, 201-216.
9 U. Tare and F. Mody, *Drilling Contractor*, 2000, 42-44.
10 A. Patel, presented in part at the SPE International Symposium on Oilfield Chemistry Houston, Texas, U.S.A., February-March, 2007.
11 R. K. Clark, R. F. Scheuerman, H. Rath and H. G. Van Laar, *J. Pet. Technol.*, 1976, **28**, 719-727.
12 B. Bloys, N. Davis, B. Smolen, L. Bailey, O. Houwen, P. Reid, J. Sherwood, L. Fraser, M. Hodder and F. Montrouge, *Oilfield Rev.*, 1994, **6**, 33-43.
13 A. Bains, E. Boek, P. Coveney, S. Williams and M. Akbar, *Mol. Simul.*, 2001, **26**, 101-145.
14 D. E. O'Brien, M. E. Chenevert, *J. Pet. Technol.,* 1973, **25**, 1089-1100.
15 G. Odriozola and J. Aguilar, *J. Chem. Theory Comput.*, 2005, **1**, 1211-1220.
16 R. L. Anderson, H. C. Greenwel, J. L. Suter, R. M. Jarvis and P. V. Coveney, *Anais da Academia Brasileira de Ciências*, 2010, **82**, 43-60.
17 R. E. Grim, Clay Mineralogy, McGraw-Hill, New York, 1900.
18 T. W. Beihoffer, presented in part at the SPE/IADC Drilling Conference, Houston, Texas, February-March, 1990.
19 C. A. Witham, J. L. Deavenport and M. K. Poindexter, US Patent 20150166868 A1, 1990.
20 A. D. Patel, presented in part at the SPE International Symposium on Oilfield Chemistry, The Woodlands. Texas, April, 2009.
21 A. D. Patel, E. Stamatakis and E. Davis, US Patent 6,247,543 B1, 2001.
22 A. Patel, E. Stamatakis, S. Young and S. Cliffe, *paper AADE*, 2002.
23 H. Zhong, Z. Qiu, W. Huang and J. Cao, *J. Pet. Sci. Eng.,* 2011, **78**, 510-515.
24 H. Zhong, Z. Qiu, D. Sun, D. Zhang and W. Huang, *J. Nat. Gas Sci. Eng.*, 2015, **26**, 99-107.
25 A. D. Patel, E. Stamatakis and E. Davis, US Patent 6609578 B2, 2003.
26 M. Garcıa, I. Ribosa, T. Guindulain, J. Sanchez-Leal and J. Vives-Rego, *Environ. Pollut.*, 2001, **111**, 169-175.
27 I. L. Shih, Y. T. Van and M. H. Shen, *Mini-Rev. Med. Chem.*, 2004, **4**, 179-188.
28 S. C. Shukla, A. Singh, A. K. Pandey and A. Mishra, *Biochem. Eng. J.*, 2012, **65**, 70-81.
29 D. Mazea, G. Schatten and W. Sale, *J Cell Biol*, 1975, **66**, 198-200.
30 Y. Guo, Y. Ma, L. Xu, J. Li and W. Yang, *J. Phys. Chem. C*, 2007, **111**, 9172-9176.
31 G. Di Stefano, F. P. Colonna, A. Bongini, C. Busi, A. Mattioli and L. Fiume, *Biochem. Pharmacol.*, 1997, **54**, 357-363.
32 J. H. Choi, S. O. Kim, E. Linardy, E. C. Dreaden, V. P. Zhdanov, P. T. Hammond and N. J. Cho, *J. Phys. Chem. B*, 2015.
33 S. Gou, T. Yin, Q. Xia and Q. Guo, *RSC Adv.,* 2015, **5**, 32064-32071.
34 M. Scholl, T. Q. Nguyen, B. Bruchmann and H. A. Klok, *J. Polym. Sci., Part A: Polym. Chem.*, 2007, **45**, 5494-5508.
35 S. W. Fox and K. Harada, *Arch. Biochem. Biophys.*, 1960, **86**, 281-285.
36 State Environmental Protection Administration, *Water and Wastewater Monitoring Analysis Method, fourth ed,* China Environmental Science Press, Beijing, 2002.
37 S. Do Jang and R. Condrate, *Clays Clay Miner.*, 1972, **20**, 79-82.
38 M. Rozenberg and G. Shoham, *Biophys. Chem.*, 2007, **125**, 166-171.
39 M. Ritz, L. Vaculikova, *Acta Geodyn. Geomater*, 2011, **8**, 47-58.
40 W. N. E. Van Dijk-Wolthuis, L. van de Water, P. van de Wetering, M. J. Van Steenbergen, J. J. Kettenes-van den Bosch, W. J. Schuyl and W. E. Hennink, *Macromol. Chem. Phys.*, 1997, **198**, 3893-3906.
41 H. Komine and N. Ogata, *Can. Geotech. J.*, 1996, **33**, 11-22.
42 D. A. Laird, *Appl. Clay Sci.*, 2006, **34**, 74-87.
43 K. Uematsu, M. Yamasaki, T. Hibi and H. Katano, *Anal. Sci.*, 2012, **28**, 657-660.
44 J. Leuba and P. Stossel, *Chitin Nat. Technol.,* 1986, 215-222.
45 T. Cardwell Jr William, US Patent 2450936 A, 1948.
46 H. He, Z. Ding, J. Zhu, P. Yuan, Y. Xi, D. Yang and R. L. Frost, *Clays Clay Miner.*, 2005, **53**, 287-293.
47 S. Belbekhouche, G. Ali, V. Dulong, L. Picton and D. Le Cerf, *Carbohydr. Polym.*, 2011, **86**, 304-312.
48 L. Quintero, *J. Dispersion Sci. Technol.*, 2002, **23**, 393-404.
49 M. Wilson and L. Wilson, *Clay Miner.,* 2014, **49**, 127-145.
50 E. Ferrage, B. Lanson, B. A. Sakharov and V. A. Drits, *Am. Mineral.*, 2005, **90**, 1358-1374.
51 R. Laura and P. Cloos, *Clays Clay Miner*, 1975, **23**, 343-348.
52 C. Blachier, L. Michot, I. Bihannic, O. Barrès, A. Jacquet and M. Mosquet, *J. Colloid Interface Sci.*, 2009, **336**, 599-606.
53 J. Cases, I. Bérend, G. Besson, M. Francois, J. Uriot, F. Thomas and J. Poirier, *Langmuir*, 1992, **8**, 2730-2739.
54 G. Jiang, Y. Xuan, Y. Li and J. Wang, *Colloid J.*, 2014, **76**, 408-415.
55 D. Zadaka, A. Radian and Y. G. Mishael, *J. Colloid Interface Sci.*, 2010, **352**, 171-177.
56 S. Anastassiadis, *Recent Pat. Biotechnol.*, 2007, **1**, 11-24.
57 Oecd, *OECD Guidelines for the Testing of Chemicals*, Organisation for Economic, 1994.
58 J. Hiraki, T. Ichikawa, S.I. Ninomiya, H. Seki, K. Uohama, H. Seki, S. Kimura, Y. Yanagimoto and J. W. Barnett, *Regul. Toxicol. Pharmacol.*, 2003, **37**, 328-340.